Effect of Hardening on the Magnetic Behavior of AISI 1045 Steel

Mario Vukotić[1], Damijan Miljavec[1], and Jaka Burja[2]

[1]Faculty of Electrical Engineering, University of Ljubljana, 1000 Ljubljana, Slovenia
[2]Institute of Metals and Technology, 1000 Ljubljana, Slovenia

Hardening is an effective method to improve the hardness of the steel construction elements of an electric machine, such as rotor shaft. Surface hardening is typically employed for shafts as it provides a material with hard wear-resistant surface (martensite) and tough and ductile core (ferrite and pearlite), with the transitional zone between them (martensite, ferrite, and pearlite). The investigations were performed on the specimens of AISI 1045 steel, which is commonly used in electric machines. There were three categories of specimens, each of them representing a region in a surface hardened shaft – normalized specimens found in as-delivered steel (core), partially hardened specimens obtained by partial hardening of normalized specimens (transitional zone), and fully hardened specimens (hardened surface), also obtained from the normalized steel. The comparison of the magnetization curves showed that partially and fully hardened specimens exhibited a decrease of saturation magnetic flux density for about 11% and 7%, respectively, compared to the normalized specimens. The magnetizing curves from this study can be directly used in the magnetic simulations of a surface-hardened shaft. This allows more accurate electromagnetic design of electric machines, in which the shaft represents an important part of the magnetic circuit, e.g., two-pole wound-rotor synchronous machine.

Index Terms— **Electric machine, hardening, hysteresis loop, magnetic properties, magnetizing curve, microstructure, shaft.**

I. Introduction

THE carbon steels with carbon content up to 1%wt., such as AISI 1000 series, are often used in electric machines as main construction elements, e.g., shafts. During the electric machine operation, a shaft has to transfer the torque and mechanical power to the load; thus, it is subjected to dynamic torsional loadings. Surface hardening enhances the shaft's ability to withstand these loads, thereby extending its lifespan. Medium carbon steels, such as 4140 (42CrMo4), 4340 (36CrNiMo4), and 1045 (C45), are commonly used for shafts due to their hardenability and toughness [1]. Shaft surface hardness is critical for ensuring the durability, reliability, and performance.

Induction surface hardening is a heat treatment process that offers several advantages for enhancing shaft surface hardness, including rapid heating, selective hardening, and minimal distortion. It is a highly effective method for achieving the desired surface hardness of the steel while maintaining a tough core. The choice of steel depends on the specific application requirements, considering factors, such as load, speed, and operating environment. The process of induction surface hardening creates a hard martensitic microstructure on the surface that transitions to a base ferritic pearlitic microstructure [2]. This means that the transitional zone consists of martensite, ferrite, and pearlite, which results in a mixture of properties. These properties have been well described in terms of mechanical characterization, especially hardness, but there is a lack of magnetic data. The latter are needed for the modeling purposes, e.g., with the finite element method, where their magnetic properties are described with a magnetization curve. Namely, the shaft, being a ferromagnetic construction element, influences the magnetic circuit of an electrical machine. However, it is often not properly included in the magnetic analyses. It is usually modeled only as air domain, leading to magnetically overdimensioned rotor designs [3]. Similar comparison of the influence of the shaft material on the magnetic properties of an electric machine was made also by Zhang et al. [4], giving the same conclusions. One of the causes for neglecting the magnetic properties of shafts might be the absence of the available data about magnetizing curves of commercially available steels.

The focus of this article is on the magnetic properties of the normalized, partially and fully hardened AISI 1045 steel, representing the microstructure types of a surface hardened shaft, more specifically the magnetizing curves, that are used in the numerical simulations of the magnetic behavior of electric machines. The literature review of this type of steel shows, that until now, the emphasis of the research has been on the influence of different heat treatment on different physical properties affecting the performance of an electrical machine, such as electrical, thermal, and mechanical properties.

Agurto et al. [5] analyzed the dependence of the electrical resistivity on the heat treatment (hardening) of 1045 steel. They established that hardening at different temperatures provoked a complex behavior, with the water-hardened specimens having higher electrical resistivity than the oil-hardened ones. Ramos et al. [6] analyzed the effects of tempering temperature on temperature-dependent thermal properties, focusing on the thermal conductivity and specific heat of 1045 steel. The former was increased by tempering, while the latter varied mildly with the different conditions of tempering. Magnabosco et al. [7] performed the analyses on the AISI 1045 steel in order to create the thermometallurgical model of the induction heat treatment, with the satisfactory agreement between the numerical and

Received 17 April 2025; revised 6 June 2025 and 5 August 2025; accepted 10 August 2025. Date of publication 13 August 2025; date of current version 26 September 2025. Corresponding author: M. Vukotić (e-mail: mario.vukotic@fe.uni-lj.si).

Color versions of one or more figures in this article are available at https://doi.org/10.1109/TMAG.2025.3598357.

Digital Object Identifier 10.1109/TMAG.2025.3598357

© 2025 The Authors. This work is licensed under a Creative Commons Attribution-NonCommercial-NoDerivatives 4.0 License.
For more information, see https://creativecommons.org/licenses/by-nc-nd/4.0/

experimental results. Zhao et al. [8] performed quasi-static combined tensile and torsional tests on normalized AISI 1045 steel. Their results showed that the ultimate tension and torsion strengths were consistent to the results of uniaxial tests, while there was some difference with the von Misses yield strength criterion. Arifin et al. [9] studied the fatigue crack propagation of 1045 steel by statistically analyzing the measured leakage magnetic flux and established correlations between the parameters and fatigue crack growth. Sayed et al. [10] studied the mechanical and microstructural properties of the gas- and shielded metal arc welded (GMAW and SMAW, respectively) thick plates of AISI 1045 steel. The plates were welded with different electrodes, and the properties of specimens were appropriate to be used in industry. Gao et al. [11] built a 3-D finite element method electromagnetic model of the spot induction hardening device in order to predict its effects on the hardness and microstructure of the 1045 steel. The simulation results were validated by the measurements. Kahrobaee et al. [12] characterized the induction hardened 1045 steel specimens with electromagnetic methods and statistical approach (principal component analysis), where the specimens had different thicknesses of hardened layers. The approach showed higher level of accuracy compared to other methods.

The magnetic properties of the 1045 steel were studied in the following papers. Jiles [13] published the results of the comprehensive research about the magnetic properties of the several AISI 1000 series steels with different carbon contents. Among others, this work offers an insight into the magnetic behavior of 1045 steel after different heat treatments, such as annealing at different temperatures for different periods of time, followed by different cooling rates. The studied magnetic properties included coercivity, permeability, remanence, and so on. Deldar et al. [14] studied the change of magnetic permeability of 1045 steel in the fatigue tests. They concluded that the measurement of the permeability represents a good non-destructive test method to evaluate the fatigue life and it can be performed during the operation. Costa et al. [15] analyzed the relationship between the 1020 and 1045 steel microstructure by non-destructive magnetic measurements, such as hysteresis and magnetic Barkhausen noise. They established that it is possible to identify the martensite and ferrite–pearlite structures by the Barkhausen noise signatures and magnetic properties. Oliveira Anício Costa et al. [16] analyzed the influence of microstructure on the electromagnetic behavior of carbon steel wires. They concluded that the electrical and mechanical behaviors heavily depend on the thermomechanical history of the material. Sahebalam et al. [17] studied the eddy current and Barkhausen noise, while assessing the heat treated (annealing, normalizing, hardening, and tempering) 1045 steel. Regression analysis was shown to be effective to accurately distinguish between the microstructures. Gorkunov et al. [18] analyzed the correlation between stress–strain state parameters and magnetic characteristics of steels St3 and 1045. They observed a direct relationship between coercivity–strain and between stress–strain on the one hand and inverse relationship between remanence–strain and between permeability–strain. Deng et al. [19] studied the effects of the structure characteristics on magnetic Barkhausen noise in commercial steels of 1000 series, i.e., steel 1045 being one of them. It was shown that Barkhausen noise parameters strongly depend on the carbon content, hardness, roughness, and elastic modulus.

In our work, the magnetic properties were measured in the form of sets of quasi-static dc hysteresis loops, from which the saturation points were extracted to form the lossless magnetization curves. The latter are commonly used in the non-linear magnetic simulations. Apart from the graphical results and photographs of the microstructure, we also added the numerical results for the magnetization curves that can be used to describe the constructional steel parts in an electric machine more accurately, as well as Vickers hardness measurement results.

II. Materials and Methods

A total of ten rod specimens of AISI 1045 (DIN C45) steel were made. The specimens were set into three categories based on the bulk microstructure throughout their volume. The first category was normalized specimens (N) with a ferritic pearlitic microstructure, usually found in as-delivered steel. The second category was partially hardened specimens (PH), where the microstructure consisted of martensite, ferrite, and minor amounts of pearlite. This is a common occurrence in the process of induction surface hardening, where the subsurface areas are not fully hardened. The third category was fully hardened specimens (FH), which consisted of a martensitic structure, typical for a fully hardened surface. The specimens were not tempered after hardening. The first four specimens N1–N4 were from the first category, the second set of specimens PH1–PH4 were from the second category, and the third set was from the third category, consisting of two specimens, FH1 and FH2. The three categories of specimens represent the layers of a surface hardened shaft–hard martensitic microstructure on the surface (specimens FH), ferritic pearlitic microstructure in the core (specimens N), and martensite, ferrite, and pearlite transitional zone between them (specimens PH).

Each rod specimen of a 100 mm length was machined by turning and brushing to the final diameter of 10.005 ± 0.001 mm. MagnetPhysik Remagraph RE3 was used to measure the quasi-static dc hysteresis loop of each specimen, following the measurement via permeameter method of IEC 60404-4 standard [20], [21]. The amplitudes of the magnetic field strength H during the measurements were set to the approximately same values for all specimens, with the maximum amplitude of around $H = 8000$ A/m. Every specimen was demagnetized prior to each measurement. Then, the excitation current was varied in order to record more than one period of magnetic field strength H (Fig. 1) and magnetic flux density B (Fig. 2). This ensures measuring a whole B–H hysteresis loop (Fig. 3) with the addition of initial magnetization (red) and finalization, when the excitation H is removed (black) and only remanent flux density B_r remains ($B_r > 0$) in the specimen.

After the measurement of each hysteresis loop, the signals of B and H were filtered to eliminate the environmental noise,

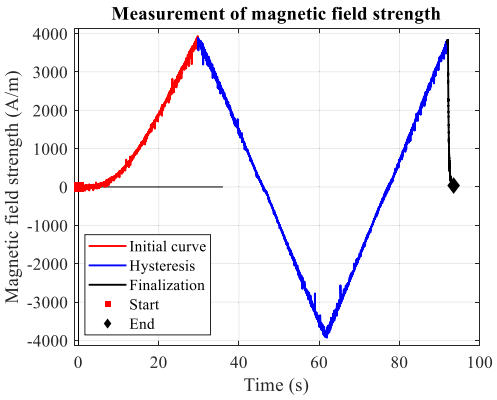

Fig. 1. Measurement of magnetic field strength.

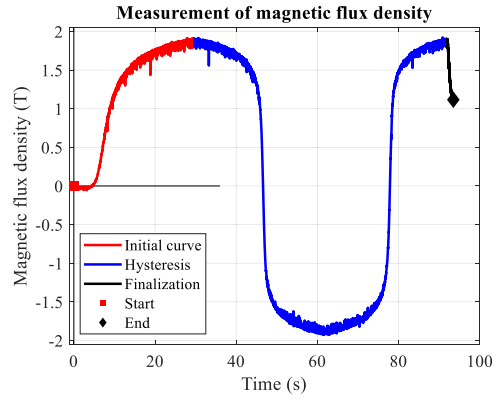

Fig. 2. Measurement of magnetic flux density.

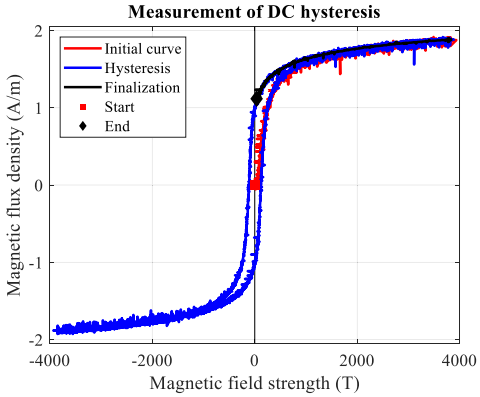

Fig. 3. Measurement of dc hysteresis loop.

captured by the Remagraph device. Then, the saturation point of the hysteresis loop was taken to form a point on the "loss-less" magnetization curve (Fig. 4), which is commonly used in the non-linear finite element method magnetic analyses, where the hysteresis and eddy-current losses of a ferromagnetic material are calculated in post-processing.

At the end of the magnetic measurements, each specimen was cut for metallographic examination. First, the specimens for metallographic analysis were ground and subsequently polished with 1 μm diamond paste. The mirror polished specimens were etched by 5% nital. The microstructures were analyzed with Nikon Microphot FXA light optical microscope.

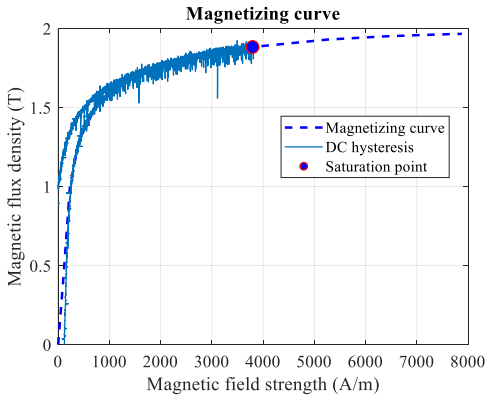

Fig. 4. Saturation point, obtained from the hysteresis loop, forming the magnetizing curve.

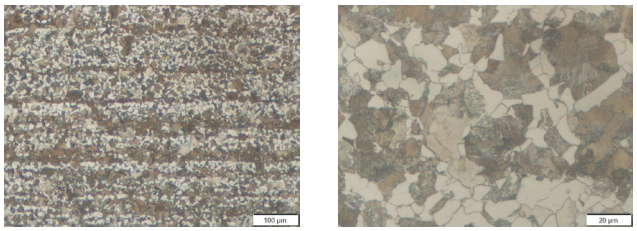

Fig. 5. First category of 1045 steel, specimen N1.

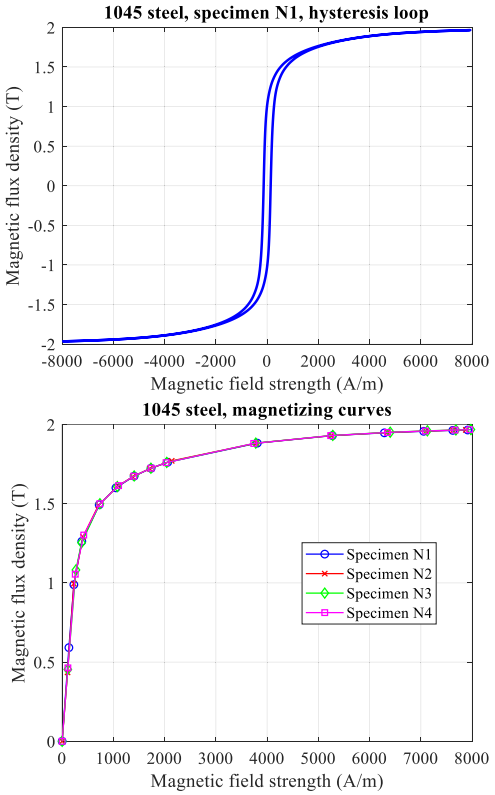

Fig. 6. Magnetic properties of the first category of 1045 steel, specimens N1–N4.

Vickers microhardness was measured using Instron Tukon 2100B microhardness tester.

TABLE I
MEASUREMENT RESULTS OF THE SPECIMENS N1–N4, SATURATION POINTS OF THE HYSTERESIS LOOPS

	Specimen N1		Specimen N2	
#	H (A/m)	B (T)	H (A/m)	B (T)
0	0	0	0	0
1	131.5	0.591	105.5	0.435
2	228.8	0.989	228.2	0.995
3	383.4	1.262	406.1	1.291
4	722.8	1.493	709.1	1.490
5	1049.6	1.600	1090.2	1.612
6	1404.4	1.674	1375.9	1.670
7	1735.4	1.723	1708.9	1.721
8	2060.0	1.762	2137.5	1.770
9	3809.0	1.882	3794.1	1.883
10	5273.8	1.930	5250.0	1.929
11	6288.1	1.947	6346.4	1.949
12	7055.5	1.957	7100.8	1.958
13	7623.1	1.963	7627.6	1.964
14	7914.5	1.965	7878.8	1.966

	Specimen N3		Specimen N4	
#	H (A/m)	B (T)	H (A/m)	B (T)
0	0	0	0.0	0
1	110.2	0.454	112.1	0.464
2	269.0	1.082	255.8	1.055
3	378.4	1.254	421.5	1.302
4	737.1	1.500	735.3	1.500
5	1077.0	1.608	1101.3	1.614
6	1405.9	1.675	1397.9	1.674
7	1731.9	1.724	1736.5	1.725
8	2041.4	1.761	2028.5	1.759
9	3778.7	1.883	3738.4	1.880
10	5281.7	1.931	5240.6	1.930
11	6402.8	1.951	6348.2	1.950
12	7127.5	1.960	7089.3	1.959
13	7683.8	1.966	7669.0	1.965
14	7977.1	1.968	7953.8	1.967

III. RESULTS AND DISCUSSION

The specimens of the first category, i.e., specimens N1–N4, exhibited the same structural and magnetic properties, shown in Figs. 5 and 6, respectively.

In Fig. 5, the normalized microstructure that consists of ferrite and pearlite, with slight banding due to solidification and hot rolling, is visible, and there is a roughly equal amount of both microstructural constituents. This kind of microstructure is typically found in 1045 steel. The core and therefore most of the volume of a shaft consist of such microstructure. Ferrite and pearlite will result in soft and relatively tough and ductile material properties. The drawback of this kind of microstructure is low wear resistance that can result in surface degradation.

In Fig. 6, the largest dc hysteresis loop of the specimen N1, obtained by one of the measurements with Remagraph RE3, is shown. The hysteresis loops of other specimens N2–N4 are the same as the one shown in Fig. 6. The saturation points for the four specimens N1–N4 are graphically shown in Fig. 6, with the numerical values given in Table I. The magnetizing curves drawn from the saturation points show identical magnetic properties of all four specimens.

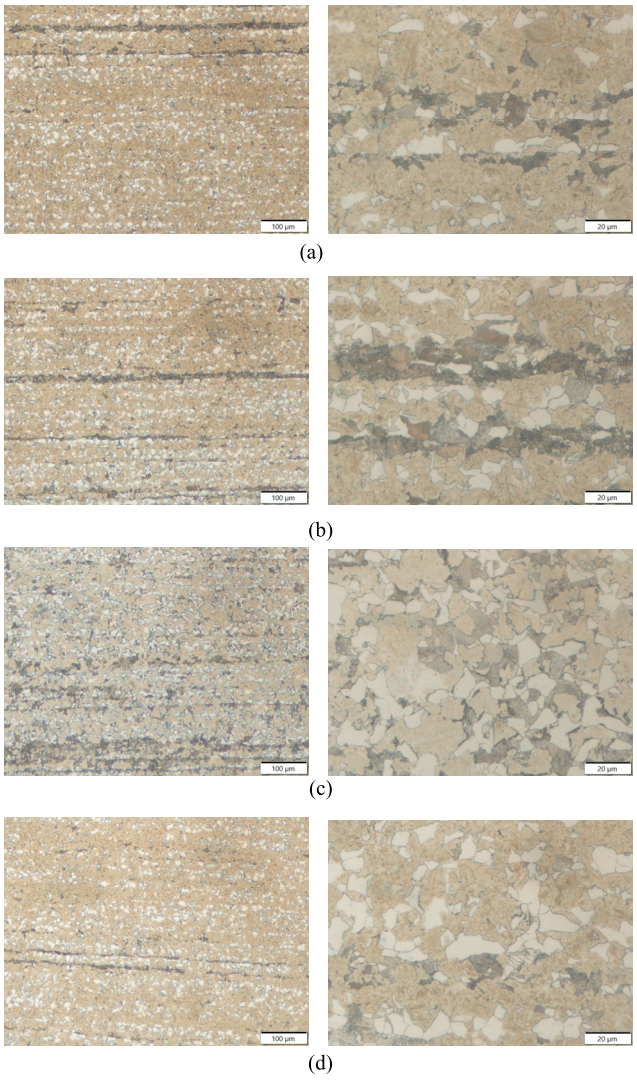

Fig. 7. Second category of 1045 steel, specimens (a) PH1, (b) PH2, (c) PH3, and (d) PH4.

The specimens of the second category, i.e., partially hardened specimens PH1–PH4, are shown in Fig. 7. The microstructures consist of martensite, ferrite, and pearlite. This is a typical microstructural composition for the subsurface transitional zone, where the microstructre transitions from fully hardened to non-affected ferrite–pearlite base microstructure. In the transitional zone, most of the ferrite is preserved beacuse it needs the highest temperature to transform to austenite. On the other hand, pearlite mostly transforms into austenite and consequently into martensite after cooling. The resulting material properties have higher hardness than the base material but not as high as the fully hardened surface. The magnetic properties of the transitional zone remain unknown due to the heterogenous chemical composition of microstructure constituence. The martensite in a fully hardened microstructure (surface) contains 0.45% C, while the martensite in the transitional zone contains approximately 0.76% C (eutectoid composition), and this causes an additional distortion of the tetragonal body-centered crystal lattice.

TABLE II
MEASUREMENT RESULTS OF THE SPECIMENS PH1–PH4, SATURATION POINTS OF THE HYSTERESIS LOOPS

	Specimen PH1		Specimen PH2	
#	H (A/m)	B (T)	H (A/m)	B (T)
0	0	0	0	0
1	172.4	0.223	139.8	0.166
2	311.2	0.437	285.2	0.384
3	311.4	0.437	440.7	0.626
4	487.5	0.723	706.9	1.037
5	721.7	1.061	1065.9	1.266
6	1158.0	1.304	1383.4	1.361
7	1448.6	1.381	1790.5	1.439
8	1784.9	1.442	2194.7	1.493
9	2073.0	1.483	3862.1	1.624
10	5116.1	1.681	5302.1	1.686
11	6291.5	1.716	6370.1	1.717
12	7027.8	1.733	7161.3	1.734
13	7583.4	1.743	7685.3	1.744
14	7897.7	1.748	7926.6	1.748
	Specimen PH3		**Specimen PH4**	
#	H (A/m)	B (T)	H (A/m)	B (T)
0	0	0	0	0
1	123.2	0.141	134.8	0.157
2	285.6	0.382	281.1	0.377
3	442.1	0.630	450.8	0.639
4	696.5	1.033	761.1	1.079
5	1077.9	1.277	1116.7	1.273
6	1325.7	1.353	1451.4	1.365
7	1704.1	1.430	1776.0	1.424
8	2022.5	1.477	2087.3	1.468
9	3728.4	1.621	3709.8	1.603
10	5210.7	1.687	5256.6	1.672
11	6299.5	1.719	6312.1	1.702
12	7064.3	1.736	7124.5	1.721
13	7626.8	1.747	7682.5	1.731
14	7904.1	1.752	7956.0	1.736

The measured magnetic properties of the specimens PH1–PH4 are almost identical (Fig. 8). The hysteresis loop is wider compared to specimens N1–N4, meaning that the coercivity increased. The remanence remained approximately the same, while the saturation point is at lower magnetic flux density. When the saturation points of measurements on all specimens PH1–PH4 are gathered together to form the magnetizing curves (Fig. 8), it can be seen that the initial permeability and saturation level are lower compared to specimens N1–N4. The knees of the magnetizing curves also occur at lower magnetic flux density and higher magnetic field strength. The numerical results are gathered in Table II. All in all, the hardening process, in which the specimens were partially hardened, resulted in worsening the magnetic properties.

The structures of the two specimens from the third category, i.e., fully hardened specimens FH1 and FH2, are shown in Fig. 9. The specimens contain untampered martensite, typically found in the surfaces of inductively hardened shafts. The high hardness provides good wear-resistance needed for parts that are exposed mechanical contact loads and friction. The martensite in these two specimens contains approximately 0.45% C, which is the bulk composition.

The coercivity and remanence points on the hysteresis loop of the specimen FH1 (Fig. 10) are similar to the points of the

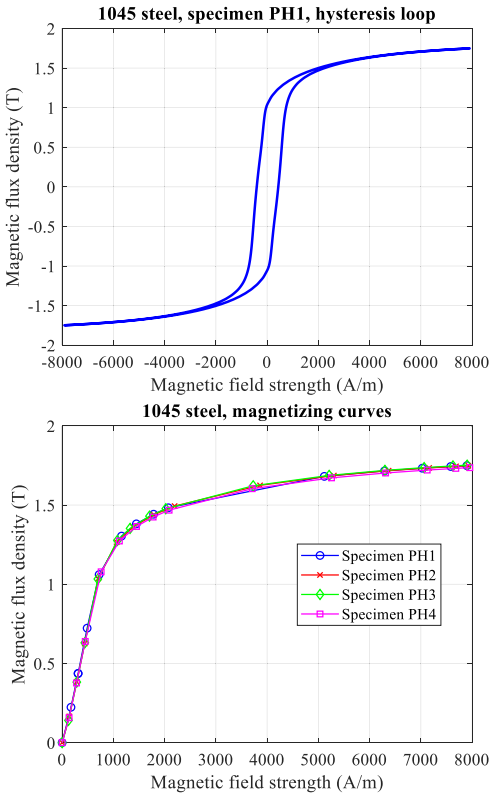

Fig. 8. Magnetic properties of second category of 1045 steel, specimens PH1–PH4.

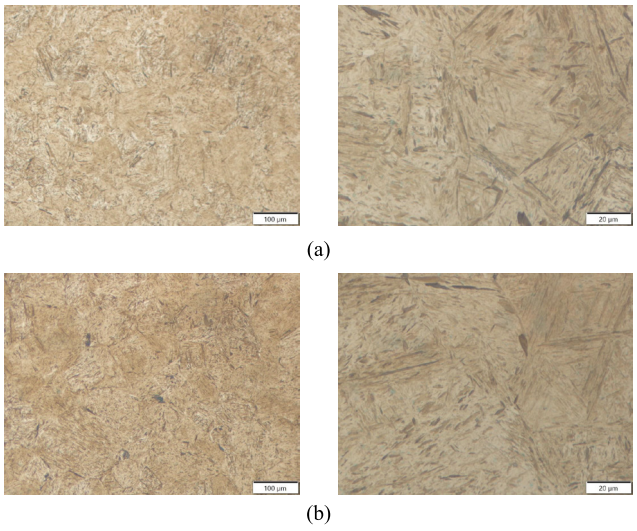

Fig. 9. Third category of 1045 steel, specimens (a) FH1 and (b) FH2.

specimens of the second category, PH1–PH4, while the saturation points are at higher magnetic flux densities (Table III). Moreover, for specimens FH1 and FH2, an additional decrease in initial permeability can be noted compared to specimens PH1–PH4.

The comparison of magnetizing curves of the specimens of different categories is shown in Fig. 11, with the other key magnetic parameters, i.e., coercivity H_c, remanence B_r, and initial relative permeability $\mu_{r,i}$, gathered in Table IV. It can be seen that hardening degrades magnetic properties of

TABLE III
MEASUREMENT RESULTS OF THE SPECIMENS FH1 AND FH2, SATURATION POINTS OF THE HYSTERESIS LOOPS

	Specimen FH1		Specimen FH2	
#	H (A/m)	B (T)	H (A/m)	B (T)
0	0	0	0.0	0.000
1	126.8	0.075	126.6	0.073
2	320.2	0.276	281.7	0.229
3	455.0	0.621	445.1	0.589
4	706.5	1.097	697.2	1.079
5	1053.0	1.306	1021.4	1.287
6	1381.7	1.408	1374.5	1.401
7	1741.5	1.483	1720.1	1.474
8	2120.3	1.541	2025.2	1.523
9	3831.7	1.695	3797.7	1.689
10	5321.2	1.764	5281.1	1.759
11	6415.3	1.797	6347.1	1.792
12	7156.0	1.815	7099.9	1.810
13	7711.7	1.825	7659.7	1.821
14	7995.5	1.830	7972.0	1.826

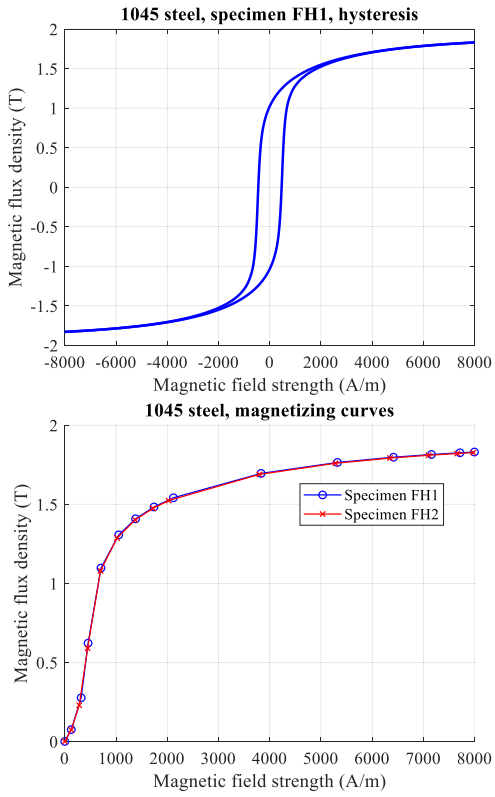

Fig. 10. Magnetic properties of third category of 1045 steel, specimens FH1 and FH2.

the 1045 steel, with partial hardening (martensite, ferrite, and pearlite in the microstructure) having a larger decrease of saturation magnetization compared to full hardening (martensite microstructure), with -11% and -7% decrease, respectively. This greater decrease in saturation magnetization is due to the presence of martensite with higher concentration of carbon. The hysteresis loops of both partially and fully hardened specimens are wider than that of the normalized material. This is a consequence of martensite formation and consequent increased dislocation density, strain, anisotropy, and internal

TABLE IV
OTHER KEY MAGNETIC PARAMETERS: COERCIVITY, REMANENCE, AND INITIAL RELATIVE PERMEABILITY

1045 steel	H_c (A/m)	B_r (T)	$\mu_{r,i}$
Normalized	136	1.018	3576
Partially hardened	420	1.047	911
Fully hardened	455	1.027	471

TABLE V
VICKERS HARDNESS MEASUREMENT RESULTS (HV10)

Specimen	N1	PH1	PH2	PH3	PH4	FH1	FH2
HV10	225	492	516	500	550	712	702

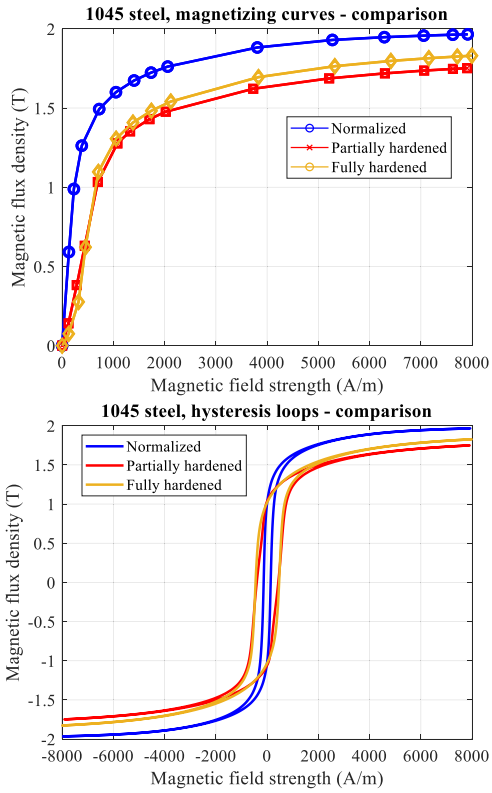

Fig. 11. Comparison of magnetizing curves and hysteresis loops of specimens that belong to different categories.

stress, all of which reduce the mobility of domain walls, thereby increasing coercivity and decreasing initial relative permeability. The variation of remanence between the three types of microstructures is minimal, as the measured values are close to one another. Additionally, in Table V, Vickers hardness (HV10) measurement results are given. The difference between the categories of specimens can be clearly seen.

IV. CONCLUSION

The magnetization curves, which were obtained by measuring the quasi-static dc hysteresis loops, can serve as the input material data for the non-linear finite-element-method magnetic simulations of a surface hardened shaft. Based on the results, presented in this article, one can apply the magnetic properties of the normalized, partially, and fully hardened 1045 steel. The normalized material shows the best magnetic

properties in terms of magnetic saturation, followed by the fully hardened and partially hardened material. This allows more accurate magnetic design and modeling, particularly in the electric machine, in which a significant portion of the magnetic flux passes the rotor shaft, e.g., two-pole wound-rotor synchronous machine.

ACKNOWLEDGMENT

This work was supported by Slovenian Research and Innovation Agency under Project L2-50084.

REFERENCES

[1] S. K. Armah, "Preliminary design of a power transmission shaft under fatigue loading using ASME code," *Amer. J. Eng. Appl. Sci.*, vol. 11, no. 1, pp. 227–244, Jan. 2018, doi: 10.3844/ajeassp.2018.227.244.

[2] U. Prisco, "Case microstructure in induction surface hardening of steels: An overview," *Int. J. Adv. Manuf. Technol.*, vol. 98, nos. 9–12, pp. 2619–2637, Oct. 2018, doi: 10.1007/s00170-018-2412-0.

[3] M. Vukotić, R. Manko, U. Rupnik, and D. Miljavec, "Magnetic modeling of shaft in an electrically-excited synchronous machine," in *Proc. 33rd Int. Electrotech. Comput. Sci. Conf.*, Sep. 2024, pp. 298–301. [Online]. Available: https://erk.fe.uni-lj.si/2024/papers/vukotic(magnetno_modeliranje).pdf

[4] W. Zhang, X. Zou, and J. Sun, "Influence of electromagnetic characteristics of shaft material on the performance of induction motor," *Int. J. Emerg. Electr. Power Syst.*, vol. 20, no. 5, pp. 1–8, Oct. 2019, doi: 10.1515/ijeeps-2019-0080.

[5] M. Q. Agurto, E. M. Atencio, F. A. R. Navarro, and J. G. M. Ramos, "Metallographic analysis and electrical resistivity of the 1045 steel after being heat-treated," *J. Met.*, vol. 27, no. 1, p. 1, 2017.

[6] N. P. Ramos, M. de Melo Antunes, A. A. A. P. da Silva, and S. M. M. de Lima E Silva, "Effects of tempering temperature on temperature-dependent thermal properties of 1045 steel," *J. Mater. Sci.*, vol. 58, no. 4, pp. 1905–1924, Jan. 2023, doi: 10.1007/s10853-022-08137-0.

[7] I. Magnabosco, P. Ferro, A. Tiziani, and F. Bonollo, "Induction heat treatment of a ISO C45 steel bar: Experimental and numerical analysis," *Comput. Mater. Sci.*, vol. 35, no. 2, pp. 98–106, Feb. 2006, doi: 10.1016/j.commatsci.2005.03.010.

[8] G. Zhao, L. Liu, D. Wang, J. Guo, and W. Chen, "Mechanical properties of AISI 1045 steel subjected to combined loads of tension and torsion," *Experim. Techn.*, vol. 42, no. 4, pp. 393–406, Aug. 2018, doi: 10.1007/s40799-018-0236-3.

[9] A. Arifin, S. Abdullah, A. K. Ariffin, N. Jamaludin, and S. S. K. Singh, "Characterising the stress ratio effect for fatigue crack propagation parameters of SAE 1045 steel based on magnetic flux leakage," *Theor. Appl. Fract. Mech.*, vol. 121, Oct. 2022, Art. no. 103514, doi: 10.1016/j.tafmec.2022.103514.

[10] A. R. Sayed et al., "Mechanical and microstructural testing of C-45 material welded by using SMAW and GMAW process," *Mater. Today, Proc.*, vol. 38, pp. 223–228, Jan. 2021, doi: 10.1016/j.matpr.2020.07.036.

[11] K. Gao et al., "Numerical and experimental analysis of 3D spot induction hardening of AISI 1045 steel," *J. Mater. Process. Technol.*, vol. 214, no. 11, pp. 2425–2433, Nov. 2014, doi: 10.1016/j.jmatprotec.2014.05.010.

[12] S. Kahrobaee, T.-H. Hejazi, and I. Ahadi Akhlaghi, "Electromagnetic methods to improve the nondestructive characterization of induction hardened steels: A statistical modeling approach," *Surf. Coatings Technol.*, vol. 380, Dec. 2019, Art. no. 125074, doi: 10.1016/j.surfcoat.2019.125074.

[13] D. C. Jiles, "Magnetic properties and microstructure of AISI 1000 series carbon steel," *J. Phys. D, Appl. Phys.*, vol. 21, no. 7, pp. 1186–1195, 1988, doi: 10.1088/0022-3727/21/7/022.

[14] S. Deldar, M. Smaga, and T. Beck, "On the influence of cyclic loadings on the magnetic permeability of ferritic-pearlitic AISI 1045 steel," *Int. J. Fatigue*, vol. 159, Jun. 2022, Art. no. 106650, doi: 10.1016/j.ijfatigue.2021.106650.

[15] L. F. T. Costa, M. F. de Campos, G. J. L. Gerhardt, and F. P. Missell, "Hysteresis and magnetic Barkhausen noise for SAE 1020 and 1045 steels with different microstructures," *IEEE Trans. Magn.*, vol. M-50, no. 4, pp. 1–4, Apr. 2014, doi: 10.1109/TMAG.2013.2287701.

[16] I. M. Oliveira Anício Costa, M. Batková, I. Batko, A. Benabou, C. Mesplont, and J.-B. Vogt, "The influence of microstructure on the electromagnetic behavior of carbon steel wires," *Crystals*, vol. 12, no. 5, p. 576, Apr. 2022, doi: 10.3390/cryst12050576.

[17] A. Sahebalam, M. Kashefi, and S. Kahrobaee, "Comparative study of eddy current and Barkhausen noise methods in microstructural assessment of heat treated steel parts," *Nondestruct. Test. Eval.*, vol. 29, no. 3, pp. 208–218, Jul. 2014, doi: 10.1080/10589759.2014.914207.

[18] E. S. Gorkunov, S. M. Zadvorkin, S. V. Smirnov, S. Y. Mitropol'skaya, and D. I. Vichuzhanin, "Correlation between the stress-strain state parameters and magnetic characteristics of carbon steels," *Phys. Met. Metallography*, vol. 103, no. 3, pp. 311–316, Mar. 2007, doi: 10.1134/s0031918x07030131.

[19] Y. Deng, Z. Li, J. Chen, and X. Qi, "The effects of the structure characteristics on magnetic Barkhausen noise in commercial steels," *J. Magn. Magn. Mater.*, vol. 451, pp. 276–282, Apr. 2018, doi: 10.1016/j.jmmm.2017.11.041.

[20] E. Steingroever and G. Ross, "Magnetic measuring techniques," Magnet-Physik Dr. Steingroever GmbH, Köln, Germany, Tech. Rep. 3055/2016, 2016.

[21] S. Tumanski, *Handbook of Magnetic Measurements*. New York, NY, USA: Taylor & Francis, 2011.

Mario Vukotić was born in 1988. He received the M.Sc. and Ph.D. degrees in electrical engineering from the University of Ljubljana, Ljubljana, Slovenia, in 2012 and 2017, respectively.

He is currently working as a Researcher with the Laboratory of Electrical Machines, Department of Mechatronics, Faculty of Electrical Engineering, University of Ljubljana. His research interests include design, analysis, and optimization of electrical machines, the different physical phenomena (electromagnetic, thermal, and mechanical) in electrical machines, and development of various custom software tools for the calculation studying of properties of electrical machines.

Damijan Miljavec (Member, IEEE) was born in 1967. He received the Ph.D. degree in electrical engineering from the University of Ljubljana, Ljubljana, Slovenia, in 1999.

He is currently working as a Full Professor with the Department of Mechatronics and the Head of the Laboratory for Electrical Machines, Faculty of Electrical Engineering, University of Ljubljana. He has co-authored several papers published in Science Citation Index (SCI) indexed scientific journals, several papers in conference proceedings, and international patents. His research interests include analysis, modeling, design, and optimization of conventional and unconventional electrical machines, design of actuators, introduction of new materials, electromagnetic compatibility (EMC) characteristics of electrical machines, and coupled analysis in electrical machines.

Jaka Burja was born in 1988. He received the M.Sc. and Ph.D. degrees in metallurgical engineering from the University of Ljubljana, Ljubljana, Slovenia, in 2012 and 2015, respectively.

He is currently working as a Researcher at the Institute of Metals and Technology, Ljubljana. His research interests include steelmaking, metallography, steel heat treatment, material properties, non-ferrous and ferrous alloys, as well as high-temperature thermodynamics.